

Scalable Hypergraph Structure Learning with Diverse Smoothness Priors

Benjamin T. Brown, Haoxiang Zhang, Daniel L. Lau, *Senior Member, IEEE*
and Gonzalo R. Arce, *Life Fellow, IEEE*

Abstract— In graph signal processing, learning the weighted connections between nodes from a set of sample signals is a fundamental task when the underlying relationships are not known a priori. This task is typically addressed by finding a graph Laplacian on which the observed signals are smooth. With the extension of graphs to hypergraphs – where edges can connect more than two nodes – graph learning methods have similarly been generalized to hypergraphs. However, the absence of a unified framework for calculating total variation has led to divergent definitions of smoothness and, consequently, differing approaches to hyperedge recovery. We confront this challenge through generalization of several previously proposed hypergraph total variations, subsequently allowing ease of substitution into a vector based optimization. To this end, we propose a novel hypergraph learning method that recovers a hypergraph topology from time-series signals based on a smoothness prior. Our approach addresses key limitations in prior works, such as hyperedge selection and convergence issues, by formulating the problem as a convex optimization solved via a forward-backward-forward algorithm, ensuring guaranteed convergence. Additionally, we introduce a process that simultaneously limits the span of the hyperedge search and maintains a valid hyperedge selection set. In doing so, our method becomes scalable in increasingly complex network structures. The experimental results demonstrate improved performance, in terms of accuracy, over other state-of-the-art hypergraph inference methods; furthermore, we empirically show our method to be robust to total variation terms, biased towards global smoothness, and scalable to larger hypergraphs.

I. INTRODUCTION

HYPERGRAPHS are considered as generalized graphs that capture higher order relationships [1]. While graphs encode pairwise relationships between nodes through edges, the higher order nature of hypergraphs extends node relations to allow an arbitrary number of nodes to be connected by a hyperedge. Figure 1 contains a sample hypergraph displaying these higher order connections. Examples of hypergraph models include email networks [2] and brain connectivity networks [3]. In the application of brain connectivity, nodes are regions of the brain specified by lobe and hemisphere, and hyperedges represent frequency bands. Any number of nodes could be connected in a hyperedge if, within the frequency

B. T. Brown, H. Zhang, and D. L. Lau are with the Department of Electrical and Computer Engineering, University of Kentucky, Lexington, KY 40506, USA.

G. R. Arce is with the Department of Electrical and Computer Engineering, University of Delaware, Newark, DE 19716, USA.

This work was partially supported by the National Science Foundation under grants 1815992 and 1816003 and the AFOSR award FA9550-22-1-0362.

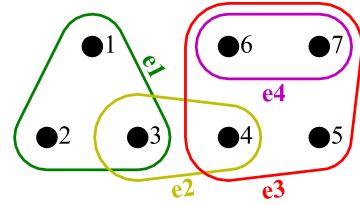


Fig. 1. Example hypergraph capturing higher order relationships. Each black circle is a node and the colored groupings are hyperedges. The hyperedges range from connecting 2 nodes to 4 nodes simultaneously.

band, there was an appropriate measurement of event-related coherence based on MEG measurements. Hypergraphs can also be used in scenarios where graphs already exist, but the relations could be extended to higher order. Examples of this lie in image processing including compression and 3-D point cloud processes [4].

While there are situations in which the choice of a network structure is naturally dependent on the application, it is not always a known quantity. Furthermore, even if a prior structure is established, it may not be optimized to the nodal relations. In such cases, the structure of the network could be recovered via learning methods. This structure recovery is of common interest with graphs and is known as graph learning or graph structure inference. Such applications of graph learning include connectome networks [5], social networks [6], and diffusion including atmospheric tracer and mobility networks [7]. Hypergraphs can be used to generalize graph learning into hypergraph learning, or hypergraph structure inference, which involves the recovery of a hypergraph structure from a set of observations, where the observations are hypergraph signals.

Some of the more prevalent and successful learning methods on traditional graphs are based on maximizing the smoothness of a set of sample signals across the graph structure where smoothness is the property describing the way a signal travels between connected nodes. At the core of recovering the topology is the concept of total variation – the measurement of this smoothness property or, more precisely, a measure of how not smooth a particular signal is where maximizing smoothness is synonymous with minimizing the signal’s total variation. To this end, Dong et al. [8] use a factor analysis model with a Gaussian probabilistic prior to introduce a method of recovering a graph Laplacian matrix that is effective on smooth

graph signals.

With inspiration from Dong et al., Kalofolias [9] developed a graph learning method based on smooth signals that infers a graph weighted adjacency matrix. Both of these methods revolve around maximizing graph signal smoothness, or equivalently, minimizing graph total variation. These works are the basis for several other graph learning related literature [10]–[12]. Furthermore, the smoothness prior is effective and abundantly used in several other graph learning contexts [13]–[16]. Reiterating that hypergraphs can be viewed as generalized graphs, it is natural that establishing a smoothness prior on hypergraph signals would be beneficial for hypergraph structure inference.

Hypergraph learning is an emerging research topic of increasing interest. Some existing works employ the use of hypergraph structure inference, oftentimes for downstream tasks. Gao et al. [17] developed a hypergraph convolution based neural network for representation learning known as HGNN+. This method uses a two step learning process where the first is modeling the hypergraph structure and the second is hypergraph convolution, which can be thought of as part of the downstream task. Gao et al. offers several hyperedge group generation options, but one in particular makes use of node features. In the node feature space, each node’s K -nearest neighbors (K -NN) are selected and formed into a hyperedge with the original node. Alternatively, the K -NN selection can be based on some maximum feature distance.

In another work, Duta and Liò [18] develop a hypergraph learning method known as SPHINX that is based on the use of multi-layer perceptrons (MLP) to iteratively produce an incidence matrix with entries being probabilities that nodes belong to hyperedges. From this, a sampling method leverages the probabilities to group nodes into hyperedges. Similarly, Bollengier et al. [19] use a deep embedded clustering method to generate the same kind of probabilistic incidence matrix for the purpose of hypergraph structure inference. All of these methods can be used with node features to learn a hypergraph structure. However, none of them make use of signal smoothness to refine their hyperedge selection.

Zhang et al. [20] propose a dynamic hypergraph learning method that alternates between updating the hypergraph incidence matrix and a label projection matrix. The problem formulation makes use of a matrix based smoothness prior on both the label projections and the node features. Another smoothness based method from Tang et al. [21] performs community detection on a line graph to form hyperedges. They use weighted Euclidean distance as total variation on a graph before proceeding to line graph construction and subsequent hypergraph structure recovery. While the methods of Zhang et al. and Tang et al. identify node signal smoothness to be of importance, the lack of uniformity of the smoothness measurement discourages judgments between which one is more effective, or if it is application dependent.

Now as with graphs, hypergraph smoothness and total variation can be referenced interchangeably with total variation referenced as the smoothness measurement. However,

there is disagreement within the hypergraph signal processing literature regarding the exact form of the total variation cost function. This diversity of smoothness measures can be attributed to the lack of a unified hypergraph signal processing framework. Consequently, there has been little work done to investigate the effects of different hypergraph total variations in structure recovery. In doing such research, this would provide insight into the validity of proposed hypergraph smoothness definitions. Case in point, Tang et al. [22] propose the hypergraph learning method Hypergraph Structure Inference Under Smoothness Prior (HGSI). The core of HGSI is a minimization problem that generates a vector-based solution capturing the hypergraph structure. Each term in the objective function controls a different aspect of the resultant hypergraph structure. Prominently discussed is the use of a smoothness prior through a total variation term limited to the metric equivalent of a sum of squared maximum differences between pairwise nodes derived by expansion of the hyperedges.

Following their outline, we propose a novel inference method that updates and improves upon the approach of HGSI in several ways. We allow our smoothness term to accommodate an assortment of total variation definitions taking into account squared and absolute differences between nodes as well as choosing the maximum difference within the set of nodes forming a hyperedge. We also update the degree positivity term to operate on a dual variable. In doing so, the closed form optimal solution of HGSI is avoided and replaced with a primal-dual algorithmic approach, which benefits in several ways including more equitable hyperedge selection. To further control the structural properties of the hypergraph, we also introduce scalar parameters to enhance or diminish the effects of certain terms such as the degree of nodes. Finally, through an investigation of the use of K -NN to reduce the number of hyperedge possibilities, we propose a method that is scalable without compromising the span of the hyperedge search. Subsequently, we avoid limiting the resulting learned structure which followed assumptions that did not always maintain a desirable set of hyperedges. Experimentally, we show our method, across the majority of scenarios and metrics, outperforms HGSI, the K -NN approach of Gao et al., and a tensor based method from Pena-Pena [23] known as PDL-HGSP.

Our work addresses limitations of prior research with the following contributions. First, we formulate a hypergraph learning model based on a smoothness prior. This model is derived from already existing graph and hypergraph learning works, however the final result is novel. We then structure the model such that a variety of smoothness, or total variation, terms can be substituted. In doing so, our work has a broader range of applications. For instance, since the optimization is robust to term substitution, our model can be fine tuned to the problem at hand with the most appropriate total variation term dependent on the desired learned structure. Furthermore, this substitution contributes to testing the efficacy of hypergraph smoothness definitions. Finally, we demonstrate why certain assumptions in previous works are undesirable and design our method to specifically avoid these issues as they relate to hyperedge selection and solution convergence. In doing so,

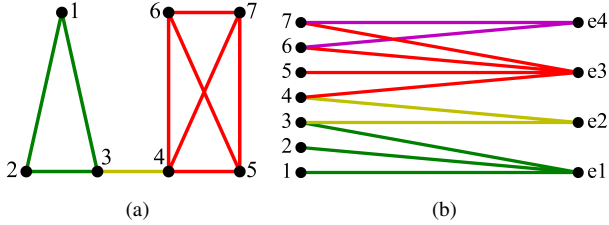


Fig. 2. Different hypergraph representations through graph expansions of the original structure in Figure 1. They are (a) clique expansion and (b) star expansion. The expansion in (a) fails to represent hyperedge \mathbf{e}_4 while (b) accurately captures it. Therefore, in the absence of \mathbf{e}_4 , the clique expansion would remain the same as in (a) while (b) would update accordingly.

our learning method becomes scalable to larger problems and adheres to a more complete view of the span of hyperedge possibilities.

II. PRELIMINARIES

A hypergraph can capture higher order relationships beyond just the pairwise. More formally, a hypergraph $\mathcal{H} = (V(\mathcal{H}), E(\mathcal{H}))$ is made up of a set of nodes $V(\mathcal{H}) = \{v_1, v_2, \dots, v_N\}$ and set of hyperedges $E(\mathcal{H}) = \{\mathbf{e}_1, \mathbf{e}_2, \dots, \mathbf{e}_Y\}$ where a hyperedge \mathbf{e}_y is a set that is allowed to connect any number of nodes simultaneously. The number of nodes is represented as $N = |V(\mathcal{H})|$, and $Y = |E(\mathcal{H})|$ is the number of hyperedges. The cardinality of a hyperedge is the number of nodes connected in the hyperedge set. The maximum cardinality M of \mathcal{H} is the largest number of nodes contained in any one hyperedge such that $\mathbf{e}_y = \{v_i, v_j, \dots, v_l : |\mathbf{e}_y| \leq M\}$ and $M \leq N$. Hyperedges may be assigned weights indicating the level of correlation between the connected nodes. Larger weights indicate higher correlation, and the system of defining correlation is application dependent.

If all the hyperedges in a hypergraph have the same cardinality, then \mathcal{H} is uniform; otherwise, it is non-uniform. Figure 1 contains an illustration of a non-uniform hypergraph with $N = 7$ and $M = 4$. Hypergraph \mathcal{H} can also be represented with an incidence matrix $\mathbf{H} \in \mathbb{R}^{N \times Y}$ where each element $H_{ij} \geq 0$. Incidence matrix \mathbf{H} can be unweighted, in which case it is a binary matrix, or weighted with scalar values between 0 and 1. If $H_{ij} > 0$, then $v_i \in \mathbf{e}_j$, otherwise $v_i \notin \mathbf{e}_j$. A hypergraph signal $\mathbf{x} = [x_1, x_2, \dots, x_N]^T \in \mathbb{R}^N$ maps each v_i to a value x_i . If there are P hypergraph signal observations, a hypergraph signal matrix $\mathbf{X} = [\mathbf{x}_1, \mathbf{x}_2, \dots, \mathbf{x}_P] \in \mathbb{R}^{N \times P}$ stores each observation column-wise. We interchangeably refer to \mathbf{X} as the hypergraph signal matrix, time-series signals, and node features.

A potential optimization framework for network inference [9], [14] is defined as

$$\min_{\mathbf{w} \in \mathcal{W}} \Omega(\mathbf{w}) + \theta(\mathbf{w}) \quad (1)$$

where \mathbf{w} is some vector from the set of valid vectors \mathcal{W} that stores the resultant structure, $\Omega(\mathbf{w})$ is the total variation term, and $\theta(\mathbf{w})$ is a term that imposes further structure on the network. Kalofolias defines \mathbf{w} to contain the weights assigned to every graph edge possibility [9]. In the context

of hypergraphs, this concept can be generalized such that $\mathbf{w} = [w_{\mathbf{e}_1}, w_{\mathbf{e}_2}, \dots, w_{\mathbf{e}_d}] \in \mathbb{R}_{\geq 0}^D$ is the vector of weights assigned to every hyperedge possibility, D . To clarify the use of D , let there be a set $\mathcal{K} = \{k_1, k_2, \dots, k_L\}$ defining all the cardinalities present in a hypergraph where each $k_l \in \mathbb{Z}^+$ is a hyperedge cardinality, and $k_l \leq M$. In the case of a hypergraph with unknown topology, but known number of nodes N and maximum cardinality M , we define

$$D = \sum_{l=1}^L \binom{N}{k_l} \quad (2)$$

such that D is the count of every possible hyperedge a hypergraph with cardinalities \mathcal{K} could have.

In graph learning, total variation $\Omega(\mathbf{w})$ has a unified definition of $\text{tr}(\mathbf{X}^T \mathbf{L} \mathbf{X})$ where $\text{tr}(\cdot)$ is the trace of a matrix, $\mathbf{X} \in \mathbb{R}^{N \times P}$ is the graph signal matrix, and $\mathbf{L} \in \mathbb{R}^{N \times N}$ is the graph Laplacian which stores the graph topology. Rewriting this such that the graph edge weight vector \mathbf{w} is the independent variable, the same as used by Kalofolias, graph total variation can be written as

$$\Omega(\mathbf{w}) = \mathbf{z}^T \mathbf{w} \quad (3)$$

where each element of the pairwise distance vector, \mathbf{z} , is $z_d = \|\mathbf{X}_{i,:} - \mathbf{X}_{j,:}\|_2^2$ and $\mathbf{X}_{i,:}^T, \mathbf{X}_{j,:}^T \in \mathbb{R}^P$ are graph time-series signals on nodes v_i and v_j , respectively, corresponding to row i and j of \mathbf{X} . In parallel, hypergraph total variation can be represented in the same way. In this case, $\mathbf{w} \in \mathbb{R}^D$ holds the hyperedge weights and $\mathbf{z} = [z_{\mathbf{e}_1}, z_{\mathbf{e}_2}, \dots, z_{\mathbf{e}_d}] \in \mathbb{R}^D$ holds some form of distance measure for each potential hyperedge. Since hyperedges are allowed to connect an arbitrary number of nodes together, the realization of the pairwise distance vector needs to be updated to a generalized distance measure. This notion has inspired several kinds of hyperedge distance definitions. With each new distance calculation stored in \mathbf{z} , there is a new hypergraph total variation measure $\Omega(\mathbf{w})$.

Nguyen and Mamitsuka [24] show that the majority of total variations have a unified form of

$$\Phi(\mathbf{X}) = T_{\mathbf{e}_d \in E(\mathcal{H})} (w_{\mathbf{e}_d} \cdot t_{v_i, v_j \in \mathbf{e}_d} (s(\mathbf{X}_{i,:}, \mathbf{X}_{j,:}))) \quad (4)$$

where $s(\mathbf{X}_{i,:}, \mathbf{X}_{j,:})$ is a kind of measure of difference between node time-series signals. The function, $t(\cdot)$, then combines these measures across all pairings of nodes $v_i, v_j \in \mathbf{e}_d$ into the distance measure which is stored in \mathbf{z} . This can then be scaled by the hyperedge weight $w_{\mathbf{e}_d}$, which is from \mathbf{w} . Finally, $T(\cdot)$ combines all measures across all hyperedges from $E(\mathcal{H})$. In its entirety, the unified smoothness term is defined as $\Phi(\mathbf{X})$. We find that the smoothness measurements we use follow the unified form of (4) and therefore are valid hypergraph total variations.

A first hypergraph total variation of interest to learning hypergraphs is the *Sum-Square* variation found in the work from Agarwal et al. [25] defined according to

$$\sum_{\mathbf{e}_d \in E(\mathcal{H})} \sum_{v_i, v_j \in \mathbf{e}_d} w_{\mathbf{e}_d} \cdot \|\mathbf{X}_{i,:} - \mathbf{X}_{j,:}\|_2^2, \quad (5)$$

which uses the squared distances between node time-series. The summations are across all pairs v_i and v_j in the hyperedge

TABLE I
CALCULATED TOTAL VARIATIONS FOR EACH PERTURBED HYPERGRAPH SIGNAL OF FIGURE 3.

Total Variation Term	No Perturbation Total Variation	Small Perturbation Total Variation	Large Perturbation Total Variation
Sum-Square	71.13	73.00	114.6
Sum-Absolute	25.36	25.45	31.78
Max-Absolute	12.80	12.80	14.47
Max-Square	44.64	44.64	62.61

of interest, e_d , and then across all hyperedges, $e_d \in E(\mathcal{H})$. When $M = 2$, this smoothness measure decomposes to the traditional means of measuring total variation in graphs, derived by either star or clique expansions. Figure 2a and 2b contain an example clique and star expansion, respectively, of the hypergraph of Fig. 1. The clique expansion is considered only as an approximation as it cannot represent non-isomorphic hypergraphs with the same clique expansion [26]. More simply, if two hypergraphs have different structures, the clique expansion could represent them in the exact same way as demonstrated in Fig. 2. The star expansion demonstrates the ability to accurately represent all hyperedges, and as such is considered a better representation.

The second hypergraph total variation of interest from Nguyen and Mamitsuka [24], noted to be associated with the clique expansion, is the *Sum-Absolute* variation defined as

$$\sum_{e_d \in E(\mathcal{H})} \sum_{v_i, v_j \in e_d} w_{e_d} \cdot \|\mathbf{X}_{i,:} - \mathbf{X}_{j,:}\|_1, \quad (6)$$

which is similar to (5) except the difference measure is now the absolute value. Both (5) and (6) sum the differences between node time-series for all $v_i, v_j \in e_d$. This property is not advantageous when combined with a minimization problem such as (1). The main issue is that as the cardinality of a hyperedge increases, there are more pairs of v_i, v_j and, therefore, more summations of time-series differences increasing the total variation. With no sort of normalization or averaging, this causes a magnitude imbalance between the contribution of hyperedges with mixed cardinalities to the overall total variation.

With the issues of (5) and (6) in mind, another hypergraph total variation is found in the work of Hein et al. [27] who propose the *Max-Absolute* variation defined by

$$\sum_{e_d \in E(\mathcal{H})} w_{e_d} \cdot \max_{v_i, v_j \in e_d} \|\mathbf{X}_{i,:} - \mathbf{X}_{j,:}\|_1, \quad (7)$$

which injects some nonlinearity by taking the maximum absolute difference between node time-series within a hyperedge. The use of the $\max(\cdot)$ difference avoids the magnitude imbalance issue and provides an interesting notion of hypergraph smoothness. This implies that the total variation contribution of a hyperedge is governed by the two nodes with the least similarity, or largest variance.

The use of the absolute difference could provide issues when it comes to a minimization problem as any perturbation to the smoothness calculation could result in changes that are too small to make a significant impact. To counteract this, we

introduce the last hypergraph total variation to be the *Max-Square* variation defined by

$$\sum_{e_d \in E(\mathcal{H})} w_{e_d} \cdot \max_{v_i, v_j \in e_d} \|\mathbf{X}_{i,:} - \mathbf{X}_{j,:}\|_2^2, \quad (8)$$

which was implemented by Tang et al. [22] and derived based on a probabilistic model with the star expansion. The introduction of the squared difference with the max term enhances the changes to the hypergraph structure more so than the absolute difference of the Max-Absolute variation.

To highlight the structural properties of each total variation term, we refer to the example of Fig. 3 where the topology of the hypergraph is the same as in Fig. 1, but here, we include a randomly generated hypergraph signal from a multivariate Gaussian distribution with mean 0 and standard deviation 2. That is to say, the signal was not designed to reflect the hyperedge connections, only to demonstrate total variation properties. We introduce changes, or perturbations, to the hypergraph signal, but only on node 5. There are three coloring representations for node 5 which correspond to the original, small perturbed, and large perturbed signals. By only perturbing node 5, we can calculate the total variation using each proposed term and observe the system response. Table I contains a report of the calculated total variation for each resultant hypergraph.

The most appropriate way of analyzing the total variations of Table I is to refer to their relative change from the original hypergraph to the perturbed hypergraphs. From the small signal change between the original and small perturbed signals, we see that only the total variation terms based on the summation of differences change while the ones based on a maximum difference remain the same. This is because node 5 is not part of the difference measure that creates the max distance between two nodes in the hyperedge. Furthermore,

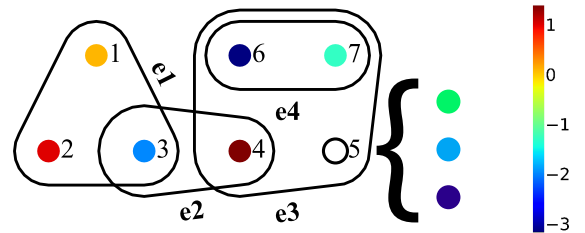


Fig. 3. Example hypergraph with perturbed signal on node 5. Colorings on node 5 from top to bottom represent: (top) no perturbation, (middle) a small perturbation, and (bottom) a large perturbation.

the small perturbation was not large enough to push node 5 into the max difference. We also note that the change in total variation using the Sum-Absolute was much smaller than the change using Sum-Square, which can be attributed to the use of a squared term versus a piecewise linear term.

Looking at the change between the original and large perturbed signals, we see much larger total variation differences caused by the larger perturbation. This time, the signal change was large enough to push node 5 into the max distance calculation which in turn caused the Max-Square and Max-Absolute total variations to increase. Furthermore, the change in total variation of the terms with square differences are once again much larger than those with absolute differences. Therefore, we can say that total variations with absolute differences will represent a signal to be smoother than those with squared distances. This is an important differentiation because these total variation terms will end up being substituted into a minimization problem. If the total variation term has a squared difference, then the optimization will be more sensitive to small changes in the input signals. However, the Max-Square total variation demonstrated a smaller change than the Sum-Square, which indicates that even among the use of squared differences, the Sum-Square will be the total variation most sensitive to signal perturbations.

III. HGSI

Tang et al. [22] proposed the hypergraph structure inference method (HGSI) to make use of the Max-Square variation, through $\Omega(\mathbf{w}) = \mathbf{z}^\top \mathbf{w}$, and includes the minimization

$$\min_{\mathbf{w}} \mathbf{z}^\top \mathbf{w} - \mathbf{1}^\top \log(\mathbf{w}) + \|\mathbf{w}\|_1, \quad (9)$$

recovering hyperedge weights, \mathbf{w} , based on a probabilistic model describing hypergraph structure and node feature relations.

The objective function for HGSI is convex with the optimal closed form solution

$$\mathbf{w}^* = \frac{1}{\mathbf{z} + 1}, \quad (10)$$

calculated element-wise on \mathbf{z} where $\mathbf{w}^* \in (0, 1]^{\hat{D}}$. The recovery of \mathbf{w}^* is the equivalent of learning the hypergraph structure since it contains the weights for each potential hyperedge, indicating how confident we are that each hyperedge is in the hypergraph. We note that the length of \mathbf{w}^* is not D , but rather \hat{D} . It is recognized that computing \mathbf{w}^* is time inefficient and, as N and M increase, often completely infeasible due to the vast number of hyperedge permutations. So, to limit the number of hyperedge possibilities, HGSI employs the use of a K-NN based method for possibility reduction. Specifically, given \mathcal{K} , determine the $k_i - 1$ nearest neighbors of each node based on time-series signal observations. Then, let the combinations of the original node and its nearest neighbors be the new set of possible hyperedges where \hat{D} is the number of hyperedge possibilities in the set reduced by K-NN.

HGSI has advantages when it comes to scalability through the use of a closed form solution and the hyperedge reduction technique. However, both of these factors also cause certain

shortcomings as they relate to assumptions on hypergraph structure. The first is that the format of (10) improperly constrains the set of learned hyperedges in a non-uniform hypergraph structure as a factor of \mathbf{z} . So, if there is some non-uniform hypergraph with hyperedges e_i and e_j , then we can say if $|e_i| < |e_j|$ and $e_i \subset e_j$, then $w_{e_j} \leq w_{e_i}$. This means that higher cardinality hyperedges will be assigned a weight that is either the same or less than the weight of some lower cardinality hyperedge subset. Therefore, if the selection of hyperedges prioritizes choosing those with the largest weights first, then the closed form solution implies that lower cardinality hyperedges could be assigned greater importance. This is an assumption that may not hold in all cases, and establishes more priors beyond that of smoothness.

The second shortcoming of HGSI is in the method of hyperedge possibility reduction. The use of K-NN provides a notion of local smoothness on the hypergraph by focusing on one node at a time and its nearest neighbors with no other outside information. While local smoothness is certainly a related concept, the use of K-NN fails to capture any global smoothness which is of greater interest when establishing a smoothness prior. This reduction method exaggerates the overlap between a hypergraph's true hyperedges and those produced by K-NN. HGSI ends up discarding valid hyperedge possibilities under the local smoothness assumption, as we will demonstrate in Sec. V.

IV. HYPERGRAPH STRUCTURE LEARNING WITH SMOOTHNESS

We now formulate our own method to recover the hypergraph structure to overcome the shortcomings of previous works. Our method, which we coin as Hypergraph Structure Learning with Smoothness (HSLs), centers around learning the weight vector $\mathbf{w} \in \mathbb{R}^D$ for an initial D hyperedge possibilities. Using the work of Tang et al. in (9) as reference, we define our total variation as $\Omega(\mathbf{w}) = \mathbf{z}^\top \mathbf{w}$. In the same experimental context, the elements of \mathbf{z} will vary depending on the smoothness term selected, but it always contains the value of the time-series difference measures. So, for the Sum-Square total variation, \mathbf{z} holds the sum of the squared differences, while for Max-Absolute, it holds the maximum of the absolute differences, and so on for the other terms. The format of $\Omega(\mathbf{w})$ provides the ability to substitute in any of the selected smoothness terms creating a robust optimization. Consequently, we can evaluate in the same setting which terms perform better. Furthermore, we reiterate that we invoke a smoothness prior for the signals on the hypergraph structure which $\Omega(\mathbf{w})$ enforces.

Revisiting the general form of (1), the use of $\theta(\mathbf{w})$ includes other terms that impose further structure on the hypergraph. We will be using a degree positivity and sparsity term in our $\theta(\mathbf{w})$. After substituting the terms into (1), the final formulation of our optimization problem is

$$\min_{\mathbf{w} \in \mathcal{W}} \mathbf{z}^\top \mathbf{w} - \alpha \mathbf{1}^\top \log(\mathbf{S}\mathbf{w}) + \beta \|\mathbf{w}\|_2^2 \quad (11)$$

where $\log(\cdot)$ is the natural logarithm taken element-wise and $\|\cdot\|_2^2$ is the squared l_2 norm of a vector. The α and β are

positive scalar parameters used to control the influence of their corresponding function. The matrix $\mathbf{S} \in \mathbb{R}^{N \times D}$ performs a linear transformation on \mathbf{w} to convert $\mathbf{S}\mathbf{w} = \mathbf{d}$. Here, $\mathbf{d} \in \mathbb{R}^N$ is the degree vector containing the degree of each node which is the sum off all the weights corresponding to hyperedges that contain v_i . Hence, the negative log term acts on degree positivity by allowing nodes to still have a degree close to zero, but remain positive. Also, since it is acting on \mathbf{d} , the α parameter can be used to control the magnitude of the node degrees. The squared l_2 norm is the sparsity term which controls the spread of the weights across the hyperedges. Similar to α , the β parameter is used to control the level of influence of sparsity on the hypergraph structure.

Here, we note the key differences between (9) and (11). First, as previously mentioned, our smoothness term is no longer fixed, but allowed to be substituted with the selected definitions. Second, the degree positivity term is now based on \mathbf{d} instead of strictly \mathbf{w} . The inclusion of \mathbf{d} is used in the tensor based hypergraph learning work of Pena-Pena et al. and the graph learning work of Kalofolias. The use of the degree vector is critical to avoid the closed form solution of (10), which in turn overcomes the issue of hyperedges being assigned unbalanced importance. Third, we change the sparsity term to be the squared l_2 norm which makes the optimization more sensitive to smaller perturbations in \mathbf{w} . Finally, we include the parameters α and β for greater control over the influence of each structural parameter.

Since our method uses \mathbf{d} , there is no longer a straightforward closed form solution like that of (10). Instead, (11) can be solved using a convex primal-dual algorithm which avoids the issue of hyperedges with varying cardinalities being assigned weighted importance. Here, it is already cast in the appropriate convex form according to Komodakis and Pesquet [28] which is

$$\min_{\mathbf{w} \in \mathcal{W}} f(\mathbf{w}) + g(\mathbf{S}\mathbf{w}) + h(\mathbf{w}) \quad (12)$$

where $h(\mathbf{w})$ must be differentiable with a positive Lipschitzian constant ζ . The terms of (11) parallel those of (12) as follows:

$$f(\mathbf{w}) = \mathbf{z}^\top \mathbf{w} + \mathbb{1}\{\mathbf{w} \geq 0\}, \quad (13)$$

$$g(\mathbf{S}\mathbf{w}) = -\alpha \mathbf{1}^\top \log(\mathbf{S}\mathbf{w}), \quad (14)$$

$$h(\mathbf{w}) = \beta \|\mathbf{w}\|_2^2. \quad (15)$$

The only new term we have introduced is the indicator function $\mathbb{1}\{\cdot\}$ where we define it as

$$\mathbb{1}\{w_i \geq 0\} = \begin{cases} 1 & , w_i \geq 0 \\ +\infty & , w_i < 0 \end{cases} \quad (16)$$

operating element-wise on \mathbf{w} . The inclusion of the indicator function is what enforces $\mathbf{w} \in \mathcal{W}$ as weights can only be non-negative real values.

From Komodakis and Pesquet, we have chosen to use the Forward-Backward-Forward (FBF) based primal-dual algorithm to perform the minimization. The FBF algorithm requires the use of the gradient of $h(\cdot)$, the proximal operator

Algorithm 1 Method of Hyperedge Reduction for HSLS

- 1: **Input:** $\mathbf{X}, \hat{\mathcal{K}}, V(\mathcal{H})$,
 - 2: **Output:** $\hat{E}(\mathcal{H}), \hat{D} = |\hat{E}(\mathcal{H})|$
 - 3: **for** $\hat{k}_l \in \hat{\mathcal{K}}$ **do**
 - 4: **for** $v_i \in V(\mathcal{H})$ **do**
 - 5: $\mathcal{J} = KNN(\mathbf{X}, v_i, \hat{k}_l)$
 - 6: Create hyperedge sets e_d from v_i combined with every unique permutation of \hat{k}_l nodes from \mathcal{J}
 - 7: Store each new e_d into reduced hyperedge set $\hat{E}(\mathcal{H})$
 - 8: **end for**
 - 9: **end for**
-

of $f(\cdot)$, and the proximal operator of the conjugate of $g(\cdot)$ denoted as $g^*(\cdot)$. These operators are defined as

$$\nabla h(\mathbf{x}) = 2\beta\mathbf{x}, \quad (17)$$

$$(\text{prox}_{\gamma f}(\mathbf{x}))_i = \max(0, x_i - \gamma z_{e_i}), \quad (18)$$

$$(\text{prox}_{\gamma g^*}(\mathbf{x}))_i = x_i - \gamma \left(\frac{y_i + \sqrt{y_i^2 + 4\alpha/\gamma}}{2} \right), \quad (19)$$

where the derivations can be found in Appendix A and B. The proximal operators are written in element-wise form to clarify how the max, square, and square root operations are being performed, and each z_{e_i} is an element from the distance vector \mathbf{z} . The γ is a constant set during the optimization process. For the proximal operator on g^* , we substituted $y_i = x_i/\gamma$.

Now, in reference to the size of the hyperedge search space, the use of D hyperedge possibilities for every potential hyperedge permutation is incredibly costly as N and the number of elements of \mathcal{K} increases. The HGSI method attempted to counteract this by reducing the hyperedge selection set using each node's $k_l - 1$ nearest neighbors. This approach is not very effective as many potential valid hyperedges are removed from consideration. We demonstrate these concepts in Sec. V where we find that, after a certain number of nearest neighbors, all hyperedges of a ground truth hypergraph are in the valid hyperedge set. So, we adopt an approach where we increase the number of nearest neighbors for each node across each cardinality k_l resulting in $\mathbf{w} \in \mathbb{R}^{\hat{D}}$ for \hat{D} number of reduced hyperedge possibilities. This method of hyperedge reduction is detailed in Algorithm 1 which operates with \mathbf{X} being the hypergraph signals across a set of nodes $V(\mathcal{H})$. From an initial set of cardinalities \mathcal{K} , the elements $\hat{k}_l \in \hat{\mathcal{K}}$ are such $\hat{k}_l \geq k_l - 1$ and represent the number of neighbors per cardinality in \mathcal{K} to keep for each node. If $\hat{k}_l = k_l - 1$, then this degrades into the exact same process as from HGSI.

We define function $KNN(\cdot)$ to produce a set of \hat{k}_l nodes that are the nearest neighbors of v_i based on Euclidean distances of the time-series in \mathbf{X} . The output $\hat{E}(\mathcal{H})$ indicates the set of all hyperedges recovered using nearest neighbors, and $\hat{D} = |\hat{E}(\mathcal{H})|$ is the number of hyperedges in the set. In our work, we have a guided method of selecting values in $\hat{\mathcal{K}}$; however, in applications without underlying hypergraph information, this selection must be based on reasonable speculation. Algorithm 1 avoids the issues of the hyperedge possibility reduction assumption of HGSI while simultaneously increasing our algorithm's scalability.

Algorithm 2 Hypergraph Structure Learning with Smoothness (HSLs): FBF Primal-Dual Algorithm for solving Equation (11).

```

1: Input:  $\alpha, \beta, \eta, \gamma$  sequence,  $i_{max}, \mathbf{z}, \mathbf{S} \in \mathbb{R}^{N \times \hat{D}}, \mathbf{w}^0 \in \mathbb{R}_{\geq 0}^{\hat{D}}, \mathbf{d}^0 \in \mathbb{R}_{\geq 0}^N$ 
2: Output:  $\mathbf{w}^{i_{end}}, \mathbf{d}^{i_{end}}$ 
3: for  $i = 0, 1, \dots, i_{max}$  do
4:   Set  $\gamma^i$ 
5:    $\mathbf{y}^i = \mathbf{w}^i - \gamma^i (\nabla h(\mathbf{w}^i) + \mathbf{S}^\top \mathbf{d}^i)$ 
6:    $\hat{\mathbf{y}}^i = \mathbf{d}^i + \gamma^i \mathbf{S} \mathbf{w}^i$ 
7:    $\mathbf{p}^i = \text{prox}_{\gamma^i f}(\mathbf{y}^i)$ 
8:    $\hat{\mathbf{p}}^i = \text{prox}_{\gamma^i g^*}(\hat{\mathbf{y}}^i)$ 
9:    $\mathbf{q}^i = \mathbf{p}^i - \gamma^i (\nabla h(\mathbf{p}^i) + \mathbf{S}^\top \hat{\mathbf{p}}^i)$ 
10:   $\hat{\mathbf{q}}^i = \hat{\mathbf{p}}^i + \gamma^i \mathbf{S} \mathbf{p}^i$ 
11:   $\mathbf{w}^{i+1} = \mathbf{w}^i - \mathbf{y}^i + \mathbf{q}^i$ 
12:   $\mathbf{d}^{i+1} = \mathbf{d}^i - \hat{\mathbf{y}}^i + \hat{\mathbf{q}}^i$ 
13:  if  $\|\mathbf{w}^{i+1} - \mathbf{w}^i\|_2^2 / \|\mathbf{w}^i\|_2^2 < \eta$  and
     $\|\mathbf{d}^{i+1} - \mathbf{d}^i\|_2^2 / \|\mathbf{d}^i\|_2^2 < \eta$  then
14:    break
15:  end if
16: end for

```

We can now define our final model for HSLs as shown in Algorithm 2. Most of the inputs are the same as those included in (11) where \mathbf{w} is the primal variable and \mathbf{d} is the dual variable. With the inclusion of Algorithm 1, we updated the appropriate dimensions with \hat{D} . The superscripts indicate which iteration of the vectors are being used as they are updated on each pass. The parameter, γ_i , is effectively the learning rate, but in every forward pass, it is updated according to a sequence determined by the Lipschitz constant, ζ . See Appendix C for details on the derivation of this sequence. The η is the threshold for the stopping condition if the max iteration i_{max} is not reached first. Following the guidelines of Komodakis and Pesquet, HSLs is guaranteed to converge.

V. EXPERIMENTS

We now evaluate the performance of our model in experimental settings¹. First, we test on co-authorship networks with both uniform and non-uniform structures. In this scenario, the underlying hypergraph structure is known and will serve as our ground truth. The purpose of this experiment is to evaluate the accuracy with which our optimization combined with various total variations can recover a hypergraph topology. The results are a report of F1-Score, Precision, and Recall between the learned hypergraph and the ground truth. Furthermore, this experiment serves to demonstrate the shortcomings of HGSI using K-NN as a method of hyperedge possibility reduction, as mentioned in Sec. III, and how that method can be improved upon. We then test on a set of lung cancer mortality data across the U.S. This experiment is designed to evaluate the effectiveness of each total variation in producing a smooth hypergraph structure. This data has no ground truth, but a

¹All source code used for our experiments is publicly available at <https://github.com/Ben-Brown-Code/Scalable-Hypergraph-Structure-Learning-with-Diverse-Smoothness-Priors>

TABLE II
NUMBER OF NODES AND HYPEREDGES FOR EXPERIMENTAL CO-AUTHORSHIP NETWORKS.

	$ V(\mathcal{H}) $	$ E(\mathcal{H}) $
DBLP (Uniform)	40	22
DBLP (Non-Uniform)	58	39
Cora (Uniform)	21	10
Cora (Non-Uniform)	61	48

comparison to a baseline hypergraph is used to highlight the emphasis our algorithm puts on selecting hyperedges that create a globally smooth topology. Finally, we use a large time-series dataset of voltage readings to test the speed and scalability of our proposed method.

A. Co-authorship Networks

We experiment on two real world co-authorship networks: DBLP and Cora [29]. For each dataset, nodes are considered authors, and a hyperedge groups nodes if the nodes' corresponding authors have written a paper together. We use a subset of the overall datasets to experiment on, and these subsets are the same that Pena-Pena et al. [23] used. Therefore, we can compare our learning method and smoothness terms to their tensor based method PDL-HGSP. We also compare results with the HGSI method from Tang et al. [22] and the K-NN approach in the node feature space from Gao et al. [17]. The experiment is performed on both a uniform and non-uniform cardinality hypergraph from both DBLP and Cora. In the uniform scenarios, the set of cardinalities $\mathcal{K} = \{3\}$. In the non-uniform scenarios, $\mathcal{K} = \{2, 3\}$. Table II details the structural parameters of the ground truth hypergraphs used.

Now, with regard to signals on the DBLP and Cora datasets, there is no given set of time-series observations. Since our method is based upon a smoothness prior, we first need to generate smooth signals across the network structures. We adopt the same process used by Tang et al. who uses a multivariate Gaussian distribution for smooth hypergraph signals, similar to processes used in graph signal processing [8]. Using the Laplacian matrix of the hypergraph star expansion \mathbf{L}_s , the signal distribution can be modeled as

$$[\mathbf{x}_V^\top, \mathbf{x}_E^\top]^\top \sim \mathcal{N}(\mathbf{0}, \mathbf{L}_s^\dagger) \quad (20)$$

where \mathbf{L}_s^\dagger is the pseudo-inverse of \mathbf{L}_s , $\mathbf{0}$ is a vector of all zeros, $\mathbf{x}_V \in \mathbb{R}^N$ is the signal across hypergraph nodes, and $\mathbf{x}_E \in \mathbb{R}^Y$ is the signal across the hyperedges. After sampling from the multivariate Gaussian distribution, we only kept \mathbf{x}_V as one hypergraph signal observation, and we stored all hypergraph signal observations in \mathbf{X} . We also add some noise along the diagonal of \mathbf{L}_s on the order of 1×10^{-3} . We note that, in this context, \mathbf{L}_s is the Laplacian of the star expansion of the ground truth hypergraphs from both the DBLP and Cora datasets and is a known quantity. We used $P = 250$ hypergraph signal observations to produce \mathbf{X} which was kept constant across all learning methods per scenario.

We started with an analysis of the overlap between the K-NN selected hyperedges and the ground truth for all co-authorship networks. Using \mathcal{K} , we selected the $k_l - 1$ nearest

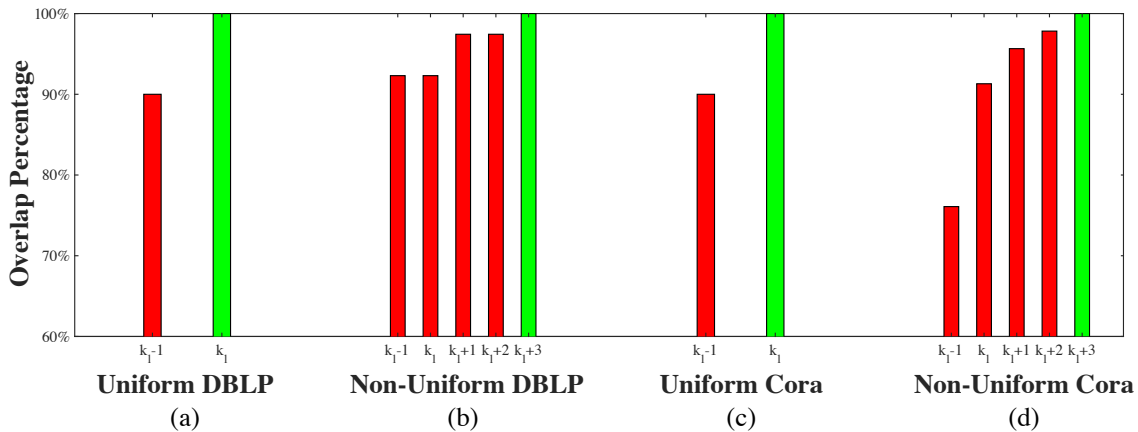


Fig. 4. Bar graphs of overlap percentage between $E_{truth}(\mathcal{H})$ and $E_{KNN}(\mathcal{H})$. Red bars indicate the percentage is less than 100%. Green bars indicate the overlap percentage has reached 100%. The x-axis is labeled in terms of the number of nearest neighbors used dependent on k_l , the cardinalities from set \mathcal{K} . Each bar plot corresponds to one of the co-authorship networkst: (a) Uniform DBLP, (b) Non-Uniform DBLP, (c) Uniform Cora, and (d) Non-Uniform Cora.

neighbors of each node from \mathbf{X} to form hyperedges. We then computed the overlap percentage between the set of ground truth hyperedges and the K-NN hyperedges. By this we mean that, for each hyperedge in the ground truth set $E_{truth}(\mathcal{H})$, we determined if it was present in the K-NN hyperedge set $E_{KNN}(\mathcal{H})$. If $E_{truth}(\mathcal{H}) \subseteq E_{KNN}(\mathcal{H})$ then this is a 100% overlap rate. We then increased the number of nearest neighbors by one and recomputed the overlap percentage for the new, larger K-NN set. This was repeated for a steadily increasing count of nearest neighbors. The computation of $E_{KNN}(\mathcal{H})$ was performed using Algorithm 1. The results are shown in the bar graphs of Fig. 4.

From the results of Fig. 4, we note that in the uniform hypergraph scenarios, the overlap percentage starts at a higher threshold than that of the non-uniform cases. This can be attributed to two main factors. The first is that the uniform scenarios have less $|E(\mathcal{H})|$ than the non-uniform scenarios. The second is that a mixed cardinality hypergraph has a much larger set of possible hyperedges making it less straightforward to select valid hyperedges. In the uniform cases, it takes significantly less neighbors in the feature space to achieve $E_{truth}(\mathcal{H}) \subseteq E_{KNN}(\mathcal{H})$ than that of the non-uniform cases. In fact, the minimum number of neighbors for this in the uniform and non-uniform scenarios is k_l and $k_l + 3$, respectively. The use of $k_l - 1$ nearest neighbors always falls below 100% overlap, demonstrating the limitation of the method of HGSI since, after the reduction of hyperedge possibilities, it is impossible for it to reproduce a hypergraph that completely corresponds to the ground truth. We also find that there is indeed a reasonable point where 100% overlap can be achieved, therefore validating our choice to incorporate a K-NN hyperedge reduction method with number of neighbors greater than $k_l - 1$. In the rest of the co-authorship network experiments, we used the corresponding number of neighbors that produced 100% overlap in Fig. 4 to reduce the size of \mathbf{w} and, consequently, \mathbf{z} .

We used \mathbf{z} , calculated from \mathbf{X} and the reduced hyperedge set, along with Algorithm 2 to get the resultant \mathbf{w} . To refine our choice of α and β , we used a hyperparameter grid search

on a log scale. The statistical results of recovering hypergraph structures for both datasets in the uniform and non-uniform scenarios can be found in Table III. A visual result of the DBLP uniform testing using HSLs can be found in Fig. 5.

We find that, in the uniform scenarios, our proposed method combined with the Max-Square total variation is always the top performer or equivalent to the best results. In the non-uniform cases, our proposed method with the Max-Square total variation produces the best F1-score and precision, but the K-NN based method of Gao et al. has the best recall. This is to be expected as recall is a measure of how many learned hyperedges are in the final result without regard to incorrect hyperedges. The use of K-NN simply recovered a larger set of hyperedges than all other methods thus increasing the chances of including a hyperedge from the ground truth. However, this is at the sacrifice of precision which explains why the F1-score is dragged down. Generally, the use of K-NN to recover the structure proves to be a reasonable approximation, especially based on the metrics of the uniform scenarios.

HSLs with the other selected total variation terms performed decent in the uniform cases, often producing better results than the compared methods. However, only the Max-Absolute total variation maintained some of this statistical response in the non-uniform case, which was a foreseen outcome discussed in Sec. II. Comparatively, HSLs with Max-Square still outperformed the other selected total variations. Since F1-score is the combination of precision and recall, it is the most apt description of overall performance. Therefore, our method was the strongest performer across the board when combined with Max-Square. We also note that all tested methods demonstrate a steep decrease in statistical output when used in a non-uniform structure application, thus demonstrating the more challenging nature of increasingly complex networks.

B. Lung Cancer Mortality Rates

From the co-authorship experiments, the evaluation metrics have demonstrated HSLs can produce reasonable results,

TABLE III
CO-AUTHORSHIP NETWORK EXPERIMENTAL METRIC RESULTS.

Learning Method	Uniform			Non-Uniform			
	F1-Score	Precision	Recall	F1-Score	Precision	Recall	
DBLP	PDL-HGSP	0.9130	0.8750	0.9545	0.7143	0.5932	0.8974
	Gao et al.	0.8000	0.7143	0.9091	0.5625	0.4045	0.9231
	HGSI	0.9091	0.9091	0.9091	0.4103	0.4103	0.4103
	HSLs with Sum-Square	0.9302	0.9524	0.9091	0.3133	0.2955	0.3333
	HSLs with Sum-Absolute	0.7458	0.5946	1.0000	0.3146	0.2800	0.3590
	HSLs with Max-Absolute	0.9048	0.9500	0.8636	0.6750	0.6585	0.6923
	HSLs with Max-Square	0.9778	0.9565	1.0000	0.8684	0.8919	0.8462
Cora	PDL-HGSP	1.0000	1.0000	1.0000	0.8000	0.7755	0.8261
	Gao et al.	0.7200	0.6429	0.8182	0.5755	0.4396	0.8333
	HGSI	0.8182	0.8182	0.8182	0.4583	0.4583	0.4583
	HSLs with Sum-Square	0.8421	0.8889	0.8000	0.4946	0.5111	0.4792
	HSLs with Sum-Absolute	0.9000	0.9000	0.9000	0.4694	0.4600	0.4792
	HSLs with Max-Absolute	0.9524	0.9091	1.0000	0.5476	0.6389	0.4792
	HSLs with Max-Square	1.0000	1.0000	1.0000	0.8478	0.8864	0.8125

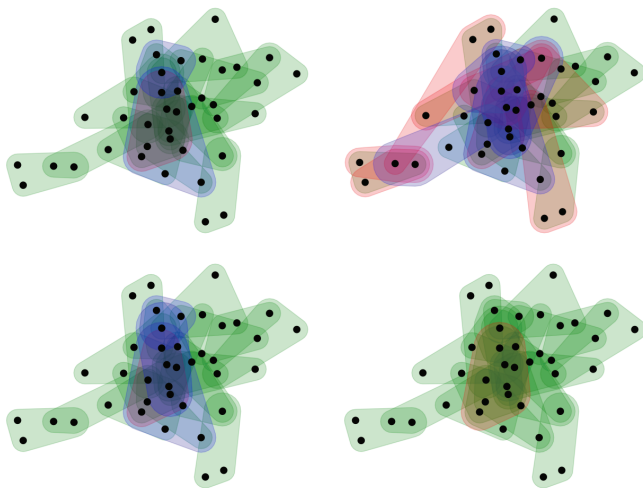


Fig. 5. Hypergraph plots of Uniform DBLP experimental results. Each hypergraph was learned with one of the four smoothness terms of interest: (top left) Sum-Square, (top right) Sum-Absolute, (bottom left) Max-Absolute, and (bottom right) Max-Square. Nodes are represented by the black circles and the learned hyperedges are the colored groupings. The hyperedges are color coded where green indicates a correctly learned hyperedge, red is an incorrectly learned hyperedge, and blue is a missing hyperedge that is in the ground truth but not the learned result.

especially in uniform cardinality applications. We now evaluate our proposed learning method on real-world data under the assertion that a smooth hypergraph structure recovery is possible with our learning algorithm. We used a dataset reporting lung cancer mortality rates on a year by year basis for each of the contiguous states in the U.S. from 2011-2019 reported in number of people per 100,000 [30]. This data is cast as a hypergraph learning problem where each state is a node and the mortality rates are the node signals. By gathering the mortality rates from all 9 years, we create a time series \mathbf{X} with $P = 9$ signal observations.

The goal is to learn a uniform hypergraph that captures a smooth structure across the nodes to evaluate the emphasis our method puts on hypergraph smoothness. To do this, we first create a baseline hypergraph using K-NN on the mortality data

to create a uniform cardinality hypergraph where $\mathcal{K} = \{3\}$. K-NN is biased towards creating hyperedges that are locally smooth, but not necessarily globally across the entire hypergraph. However, as we previously investigated with the co-authorship networks, K-NN selected hyperedges can produce reasonable approximations of globally smooth hypergraphs. To that end, we used each of the four proposed total variations on the baseline K-NN hypergraph structure. Then, we used HSLs to recover hypergraphs with the mortality data. We then calculated the corresponding total variation of our learned hypergraphs for comparison with the baseline. The idea here is that the baseline hypergraph should be relatively smooth, due to K-NN local properties, but our method should encourage better results that are globally smooth. Since the magnitude of the total variation calculations are dependent on the number of hyperedges, we constrain our optimization to have at least as many hyperedges as the baseline.

To further demonstrate the experimental smoothness properties, we introduced two other datasets. The first contains smoking rates [31] and the second contains temperature readings [32]. Both datasets are reported on a year by year basis from 2011-2019 and are therefore of a similar format to the mortality data. We then used the hypergraph structure learned on the mortality data to calculate the corresponding total variation with the smoking and temperature readings. It is well known that the onset of lung cancer and smoking are certainly correlated factors [33]. Furthermore, the correlation between lung cancer and temperature is at best ambiguous, but certainly not as strong as smoking. To demonstrate this idea, Fig. 6 contains color maps of the U.S. based on average lung cancer mortality (Fig. 6 left), average smoking rates (Fig. 6 middle), and average temperature (Fig. 6 right) across the year. The data has been normalized so the figures are on comparable scales. Visually, it is clear that the coloring of the mortality and smoking maps share similar trends, especially in the southeast and northeast regions. These trends become less similar when comparing these two maps to the temperature map which gradients across the U.S. from north to south. So, we expect that if our method can successfully learn a smooth

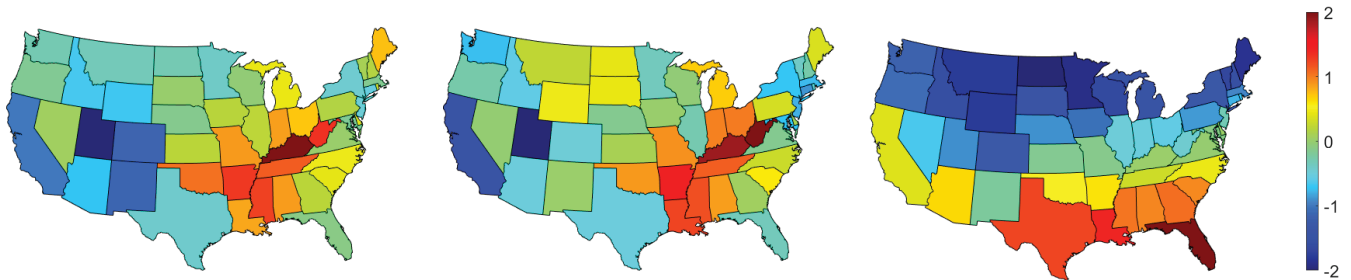


Fig. 6. Color maps of data on the contiguous U.S. map. The corresponding datasets are: (left) mortality, (middle) smoking, (right) temperature. All data is averaged across the 2011-2019 observations. The color-bar represents the separately normalized z-score for each dataset.

TABLE IV
RESULTS OF UNIFORM HYPERGRAPH LEARNING USING THE STRUCTURE RECOVERED FROM MORTALITY DATA.

	Sum-Square	Sum-Absolute	Max-Absolute	Max-Square
K-NN Total Variation	59.3	148.5	63.0	28.5
K-NN \mathcal{E}	32	32	32	32
HSLs Total Variation	41.9	142.7	60.4	11.5
HSLs \mathcal{E}	38	32	32	34
Smoking Total Variation	305.5	431.1	206.1	162.0
Temperature Total Variation	2006.7	922.2	500.3	1184.6

hypergraph on the mortality data, then correlated factors, such as smoking rates, would also be approximately smooth on the same structure. We also expect that factors uncorrelated to the mortality data, such as temperature, should be less smooth across the structure than that of the correlated factors. The results of using K-NN, the learned hypergraphs, and correlated factors are all reported in Table IV.

HSLs, when compared with the baseline K-NN learned hypergraph, always produced smoother structures on the mortality data, even in the presence of more hyperedges. The Sum-Square and Max-Square total variations generate the largest disparity between the baseline and the algorithmic total smoothness measure, which aligns with the discussion of the total variation structural properties in Sec. II. Furthermore, we note that during the learning process, the sets of hyperedges learned by K-NN and HSLs always had overlap. This makes sense as K-NN promotes local smoothness which can occasionally be optimal for global smoothness as well. The total variation using the smoking data is across the board much greater than that of the baseline and algorithmic approaches. However, comparing the metrics of the smoking and temperature data, we find that the correlated smoking signal was always significantly smoother on the original hypergraph than the less correlated temperature. Therefore, we believe that the learned hypergraph could be used to distinguish between potentially correlated and uncorrelated variables to the initial

dataset.

C. Voltage Meter Readings

Thus far, our experiments have demonstrated HSLs to be accurate and globally smooth, specifically when paired with Max-Square variation. From this basis, we now establish our method to also be fast and scalable. Here, a synthetic time-series dataset has been simulated and generated using OpenDSS [34] software on an IEEE34 power circuit, which is a standard test feeder circuit simulating a power distribution system [35]. The dataset is comprised of 95 nodes with over 2000 hourly samples. Each node in the time-series represents a node on the feeder circuit where voltage magnitude has been measured with the help of a smart meter or an Advanced Metering Infrastructure (AMI) [36]. Each of these signals have been assigned a phase A, B, or C with phases differing from each other by 120 degrees. Therefore, this dataset is suitable for clustering problems based upon phase identification where nodes with similar signals are expected to be from the same phase grouping. It is imperative to assign accurate phase labels in order to avoid the situation of an unbalanced three-phase load being delivered to customers.

We experiment on this synthetic data by applying the HSLs with Max-Square variation to demonstrate the scalability and speed with which a hypergraph can be learned on a larger dataset. Previously, we have tested on datasets ranging from 21 to 61 nodes and a maximum cardinality not exceeding $M = 3$. Now, we have a much larger 95 node dataset where we learn a uniform hypergraph ranging from $M = 3$ to $M = 6$. We also set $\hat{\mathcal{K}} = \{10\}$ for Algorithm 1 for each learned hypergraph. Table V reports the time in seconds that Algorithm 1 and Algorithm 2 took to run.

We see that the largest time dependency is on the selection of the valid hyperedge set. While this may seem constraining, due to the nature of the learning problem, Algorithm 1 needs to only run once while the hypergraph topology is expected to remain static. Therefore, after the initial creation of the hyperedge selections, the only time constraint is on Algorithm 2 which, even in high cardinality scenarios, remains under 750ms runtime. Determining a fast speed is certainly application dependent, however, in this particular scenario, these times are acceptable as the observations are taken hourly, meaning our method has learned the hypergraph well before the next set of observations are completed.

TABLE V
TIME RESULTS OF UNIFORM HYPERGRAPH LEARNING USING VOLTAGE
METERING.

	$M = 3$	$M = 4$	$M = 5$	$M = 6$
Algorithm 1 Time (s)	8.62	56.19	161.21	220.98
Algorithm 2 Time (s)	0.15	0.44	0.68	0.74

Learning a hypergraph with $M = 6$ demonstrates the scalability of our method. Hypergraph inference is slowed by the increase of N and M , but here we show that HSLs can handle such a change. For reference, in the least complex scenario of $M = 3$, if a method is based on using every hyperedge possibility, this already exceeds our software’s maximum allowable variable memory size. This issue only intensifies as you increase the maximum cardinality. In general, the worst case space complexity for generating all hyperedge possibilities is $\mathcal{O}(N \cdot \binom{N-1}{k_{max}} \cdot k_{max})$ where k_{max} is the cardinality that results in the largest value for $\binom{N-1}{k_{max}}$. Our method overcomes this barrier with the use of Algorithm 1 and scales to several cardinalities higher by reducing the worst space complexity to be $\mathcal{O}(N \cdot \max_l \binom{\hat{k}_l}{k_l} \cdot k_l)$ where the main term that achieves this reduced complexity is \hat{k}_l which can be significantly less than the previously used $N - 1$.

VI. CONCLUSION

In this paper, we developed a hypergraph learning optimization method, HSLs, where we aimed to overcome shortcomings of previous works including the lack of a smoothness prior, broad usage of total variation, and algorithmic assumptions. We overcame the first two problems by basing our optimization framework on minimizing the total variation while allowing the smoothness term to be robust for substitution. The choice to format our optimization with a primal and dual variable and the investigation into the use of K-NN as a means of hyperedge possibility reduction solved the issues surrounding the algorithmic assumptions related to weighted hyperedge importance and valid hyperedge search spaces. Furthermore, the K-NN reduction method we improved upon made our method scalable without compromising the span of the hyperedge search. We were able to experimentally evaluate the effectiveness of our proposed method, with each selected total variation, in recovering a hypergraph structure based on the smoothness prior.

When investigating our method’s ability to accurately recover a hypergraph compared against the ground truth topology, we found that our proposed method HSLs with the Max-Square was the overall best performer when compared to the other smoothness terms and the results of other methods. This validated our optimization framework showing that reasonable hypergraph structure recovery was possible and total variation substitution was viable. We proceeded with evaluating how well our method performed on encouraging a smooth hypergraph structure. We found that across all total variations, our method encouraged global smoothness more so than the K-NN baseline. We also determined that our method recovers a

structure that is smoother across data correlated to the original dataset and less smooth across uncorrelated data, highlighting a key property of the learned hypergraph structure. Finally, we demonstrated our method’s ability to scale to larger problems with more nodes and significantly larger maximum cardinalities. We also determined that the main time dependence was on the hyperedge reduction algorithm, but this was of little issue as the expectation is to complete that process only once per static application.

In future work, we will extend concepts to a dynamic domain where time-series data is subject to alter as more observations are taken and where the hypergraph structure at one point in time may not be consistent with future points in time. We believe that our work here is a suitable starting point to evolve the research in this direction.

ACKNOWLEDGEMENT

The authors would like to thank Mihir Malladi for their contribution to the work in regard to some of the experimental data acquisition and interpretation.

APPENDIX A PROOF OF EQUATION (18)

First, we write out the definition of the proximal operator as

$$\text{prox}_{\gamma f}(\mathbf{x}) := \underset{\mathbf{u}}{\text{argmin}} f(\mathbf{u}) + \frac{1}{2\gamma} \|\mathbf{u} - \mathbf{x}\|_2^2. \quad (21)$$

Using the proximal affine addition operation, we establish that if you have the problem of the form $\hat{f}(\mathbf{x}) = \Psi(\mathbf{x}) + \mathbf{a}^\top \mathbf{x} + \mathbf{b}$, then

$$\text{prox}_{\gamma \hat{f}}(\mathbf{x}) = \text{prox}_{\gamma \Psi}(\mathbf{x} - \gamma \mathbf{a}) \quad (22)$$

for some function $\Psi(\mathbf{x})$ and constant vectors \mathbf{a}, \mathbf{b} . We can directly apply the original function $f(\mathbf{x}) = \mathbf{z}^\top \mathbf{x} + \mathbb{1}\{\mathbf{x} \geq 0\}$ where $\Psi(\mathbf{x}) = \mathbb{1}\{\mathbf{x} \geq 0\}$, $\mathbf{a} = \mathbf{z}$, and $\mathbf{b} = \mathbf{0}$. Using the proximal rule of (22), we can write

$$\text{prox}_{\gamma f}(\mathbf{x}) = \text{prox}_{\gamma \mathbb{1}\{\cdot\}}(\mathbf{x} - \gamma \mathbf{z}), \quad (23)$$

and substituting into the proximal operator definition of (21) we arrive at

$$\begin{aligned} \text{prox}_{\gamma \mathbb{1}\{\cdot\}}(\mathbf{x} - \gamma \mathbf{z}) = \\ \underset{\mathbf{u}}{\text{argmin}} \mathbb{1}\{\mathbf{u} \geq 0\} + \frac{1}{2\gamma} \|\mathbf{u} - (\mathbf{x} - \gamma \mathbf{z})\|_2^2. \end{aligned} \quad (24)$$

With the indicator function, we note that the argument $\mathbf{u} \geq 0$ is the definition of the indicator function set C meaning that if the argument satisfies the condition, then that argument is in set C . Since the proximal operator is being performed on the indicator function, this is considered the projection of \mathbf{u} onto C which allows the rewrite of (24) as

$$\text{prox}_{\gamma \mathbb{1}\{\cdot\}}(\mathbf{x} - \gamma \mathbf{z}) = \underset{\mathbf{u} \in C}{\text{argmin}} \|\mathbf{u} - \mathbf{x} + \gamma \mathbf{z}\|_2^2 \quad (25)$$

where we also discarded the $1/2\gamma$ constant that no longer affects the result. We now have the constraint that $\mathbf{u} \in C$. We proceed with minimizing via the gradient as

$$\nabla \|\mathbf{u} - \mathbf{x} + \gamma \mathbf{z}\|_2^2 = 2(\mathbf{u} - \mathbf{x} + \gamma \mathbf{z}). \quad (26)$$

Then, setting (26) to $\mathbf{0}$ the result is

$$\mathbf{u} = \mathbf{x} - \gamma \mathbf{z}. \quad (27)$$

The final step is to include the constraint $\mathbf{u} \in C$. We know that u_i remains unchanged if it is negative, otherwise it is set to $+\infty$. So, we can threshold out the negative values and arrive at

$$(\text{prox}_{\gamma \mathbb{1}\{\cdot\}}(\mathbf{x} - \gamma \mathbf{z}))_i = \max(0, x_i - \gamma z_i), \quad (28)$$

which, when substituting using (23), provides exactly the answer in (18).

APPENDIX B PROOF OF EQUATION (19)

We first introduce the general form of the Moreau Decomposition as

$$\mathbf{x} = \text{prox}_{\gamma g}(\mathbf{x}) + \gamma \text{prox}_{g^*/\gamma}(\mathbf{x}/\gamma). \quad (29)$$

Using function $g(\mathbf{x}) = -\alpha \mathbf{1}^\top \log(\mathbf{x})$, it is well established for the logarithmic barrier that

$$(\text{prox}_{\gamma g}(\mathbf{x}))_i = \frac{x_i + \sqrt{x_i^2 + 4\alpha\gamma}}{2}, \quad (30)$$

which is written in its element-wise form for $i = 1, 2, \dots, n$ where $\mathbf{x} \in \mathbb{R}^n$. Here, we establish that the logarithmic barrier g is convex and closed, and as such the conjugate of the conjugate function produces the original function $(g^*)^* = g$. With this in mind, we can rewrite (29) as

$$\text{prox}_{\gamma g}(\mathbf{x}) = \mathbf{x} - \gamma \text{prox}_{g^*/\gamma}(\mathbf{x}/\gamma). \quad (31)$$

Rewriting the functions to be their conjugates and substituting in (30), we get

$$(\text{prox}_{\gamma g^*}(\mathbf{x}))_i = x_i - \gamma (\text{prox}_{g/\gamma}(\mathbf{x}/\gamma))_i \quad (32)$$

$$= x_i - \gamma \left(\frac{x_i/\gamma + \sqrt{(x_i/\gamma)^2 + 4\alpha/\gamma}}{2} \right) \quad (33)$$

$$= x_i - \gamma \left(\frac{y_i + \sqrt{y_i^2 + 4\alpha/\gamma}}{2} \right) \quad (34)$$

where, after replacing $x_i/\gamma = y_i$, we get exactly (19).

APPENDIX C DERIVATION OF LEARNING RATE SEQUENCE γ

The learning rate sequence γ is dependent on the Lipschitz constant ζ of h from (12). This constant is the minimum value of

$$\|\nabla h(\mathbf{x}) - \nabla h(\mathbf{y})\| \leq \zeta \|\mathbf{x} - \mathbf{y}\| \quad (35)$$

where $\zeta \in \mathbb{R}^+$. Substituting ∇h from (17), we can rewrite (35) as

$$\|2\beta \mathbf{x} - 2\beta \mathbf{y}\| \leq \zeta \|\mathbf{x} - \mathbf{y}\|. \quad (36)$$

Then, we pull out the constant 2β and divide both sides by $\|\mathbf{x} - \mathbf{y}\|$ to get $2\beta \leq \zeta$. Since the Lipschitz constant is supposed to be the minimum value, then $\zeta = 2\beta$.

From here, there is no longer any derivation, only the definition of the sequence of γ defined by

$$\mu = \zeta + \|S\|_s, \quad (37)$$

$$\epsilon \in (0, 1/(1 + \mu)), \quad (38)$$

$$(\gamma_n)_{n \in \mathbb{N}} \in [\epsilon, (1 - \epsilon)/\mu] \quad (39)$$

where $\|\cdot\|_s$ is the spectral norm, ϵ is some scalar, and each γ in the sequence is indexed by n .

REFERENCES

- [1] Y. Gao, Z. Zhang, H. Lin, X. Zhao, S. Du, and C. Zou, "Hypergraph learning: Methods and practices," *IEEE Transactions on Pattern Analysis and Machine Intelligence*, vol. 44, no. 5, pp. 2548–2566, 2022.
- [2] I. Amburg, J. Kleinberg, and A. R. Benson, "Planted hitting set recovery in hypergraphs," *Journal of Physics: Complexity*, vol. 2, no. 3, p. 035004, may 2021. [Online]. Available: <https://dx.doi.org/10.1088/2632-072X/abdb7d>
- [3] A. N. Pisarchik, N. P. Serrano, and R. Jaimes-Reátegui, "Brain connectivity hypergraphs," in *2024 8th Scientific School Dynamics of Complex Networks and their Applications (DCNA)*, 2024, pp. 190–193.
- [4] S. Zhang, S. Cui, and Z. Ding, "Hypergraph-based image processing," in *2020 IEEE International Conference on Image Processing (ICIP)*, 2020, pp. 216–220.
- [5] O. Sporns, "Structure and function of complex brain networks," *Dialogues in Clinical Neuroscience*, vol. 15, no. 3, pp. 247–262, 2013, pMID: 24174898. [Online]. Available: <https://doi.org/10.31887/DCNS.2013.15.3/osporns>
- [6] G. Mateos, S. Segarra, and A. Marques, "Chapter 13 - inference of graph topology," in *Cooperative and Graph Signal Processing*, P. M. Djurić and C. Richard, Eds. Academic Press, 2018, pp. 349–374. [Online]. Available: <https://www.sciencedirect.com/science/article/pii/B9780128136775000134>
- [7] D. Thanou, X. Dong, D. Kressner, and P. Frossard, "Learning heat diffusion graphs," *IEEE Transactions on Signal and Information Processing over Networks*, vol. 3, no. 3, pp. 484–499, 2017.
- [8] X. Dong, D. Thanou, P. Frossard, and P. Vandergheynst, "Learning laplacian matrix in smooth graph signal representations," *IEEE Transactions on Signal Processing*, vol. 64, no. 23, pp. 6160–6173, 2016.
- [9] V. Kalofolias, "How to learn a graph from smooth signals," in *Proceedings of the 19th International Conference on Artificial Intelligence and Statistics*, ser. Proceedings of Machine Learning Research, A. Gretton and C. C. Robert, Eds., vol. 51. Cadiz, Spain: PMLR, 09–11 May 2016, pp. 920–929. [Online]. Available: <https://proceedings.mlr.press/v51/kalofolias16.html>
- [10] H. E. Egilmez, E. Pavez, and A. Ortega, "Graph learning from data under laplacian and structural constraints," *IEEE Journal of Selected Topics in Signal Processing*, vol. 11, no. 6, pp. 825–841, 2017.
- [11] R. Balestrierio and Y. LeCun, "Contrastive and non-contrastive self-supervised learning recover global and local spectral embedding methods," in *Advances in Neural Information Processing Systems*, S. Koyejo, S. Mohamed, A. Agarwal, D. Belgrave, K. Cho, and A. Oh, Eds., vol. 35. Curran Associates, Inc., 2022, pp. 26 671–26 685. [Online]. Available: https://proceedings.neurips.cc/paper_files/paper/2022/file/aa56c74513a5e35768a11f4e82dd7ffb-Paper-Conference.pdf
- [12] S. Segarra, A. G. Marques, G. Mateos, and A. Ribeiro, "Network topology inference from spectral templates," *IEEE Transactions on Signal and Information Processing over Networks*, vol. 3, no. 3, pp. 467–483, 2017.
- [13] S. Chepuri, S. Liu, G. Leus, and A. Hero, "Learning sparse graphs under smoothness prior," in *2017 IEEE International Conference on Acoustics, Speech, and Signal Processing - Proceedings*. United States: IEEE, 2017, pp. 6508–6512, iCASSP 2017 : 42nd IEEE International Conference on Acoustics, Speech and Signal Processing - The Internet of Signals, ICASSP ; Conference date: 05-03-2017 Through 09-03-2017. [Online]. Available: <http://www.ieee-icassp2017.org/>
- [14] S. S. Saboksayr, G. Mateos, and M. Cetin, "Online graph learning under smoothness priors," *2021 29th European Signal Processing Conference (EUSIPCO)*, 2021. [Online]. Available: <https://par.nsf.gov/biblio/10321463>
- [15] V. Kalofolias and N. Perraudin, "Large scale graph learning from smooth signals," in *International Conference on Learning Representations*, 2019. [Online]. Available: <https://openreview.net/forum?id=ryGkSo0qYm>

- [16] M. G. Rabbat, “Inferring sparse graphs from smooth signals with theoretical guarantees,” in *2017 IEEE International Conference on Acoustics, Speech and Signal Processing (ICASSP)*, 2017, pp. 6533–6537.
- [17] Y. Gao, Y. Feng, S. Ji, and R. Ji, “Hgnn+: General hypergraph neural networks,” *IEEE Transactions on Pattern Analysis and Machine Intelligence*, vol. 45, no. 3, pp. 3181–3199, 2023.
- [18] I. Duta and P. Liò, “Sphinx: Structural prediction using hypergraph inference network,” 2024. [Online]. Available: <https://arxiv.org/abs/2410.03208>
- [19] M. Bollengier, A. A. Díaz Berenguer, and H. Sahli, “Dynamic multi-hypergraph structure learning for disease diagnosis on multimodal data,” in *2024 46th Annual International Conference of the IEEE Engineering in Medicine and Biology Society (EMBC)*, 2024, pp. 1–5.
- [20] Z. Zhang, H. Lin, and Y. Gao, “Dynamic hypergraph structure learning,” in *Proceedings of the 27th International Joint Conference on Artificial Intelligence*, ser. IJCAI’18. AAAI Press, 2018, p. 3162–3169.
- [21] B. Tang, S. Chen, and X. Dong, “Learning hypergraphs from signals with dual smoothness prior,” in *ICASSP 2023 - 2023 IEEE International Conference on Acoustics, Speech and Signal Processing (ICASSP)*, 2023, pp. 1–5.
- [22] B. Tang, S. Chen, and X. Dong, “Hypergraph Structure Inference From Data Under Smoothness Prior,” *arXiv e-prints*, p. arXiv:2308.14172, Aug. 2023.
- [23] K. Pena-Pena, L. Taipe, F. Wang, D. L. Lau, and G. R. Arce, “Learning hypergraphs tensor representations from data via t-hgsp,” *IEEE Transactions on Signal and Information Processing over Networks*, vol. 10, pp. 17–31, 2024.
- [24] H. C. Nguyen and H. Mamitsuka, “Learning on hypergraphs with sparsity,” *IEEE Transactions on Pattern Analysis and Machine Intelligence*, p. 1–1, 2020. [Online]. Available: <http://dx.doi.org/10.1109/TPAMI.2020.2974746>
- [25] S. Agarwal, K. Branson, and S. Belongie, “Higher order learning with graphs,” in *Proceedings of the 23rd International Conference on Machine Learning*, ser. ICML ’06. New York, NY, USA: Association for Computing Machinery, 2006, p. 17–24. [Online]. Available: <https://doi.org/10.1145/1143844.1143847>
- [26] K. Hayashi, S. G. Aksoy, C. H. Park, and H. Park, “Hypergraph random walks, laplacians, and clustering,” in *Proceedings of the 29th ACM International Conference on Information & Knowledge Management*, ser. CIKM ’20. New York, NY, USA: Association for Computing Machinery, 2020, p. 495–504. [Online]. Available: <https://doi.org/10.1145/3340531.3412034>
- [27] M. Hein, S. Setzer, L. Jost, and S. S. Rangapuram, “The total variation on hypergraphs - learning on hypergraphs revisited,” in *Proceedings of the 27th International Conference on Neural Information Processing Systems - Volume 2*, ser. NIPS’13. Red Hook, NY, USA: Curran Associates Inc., 2013, p. 2427–2435.
- [28] N. Komodakis and J.-C. Pesquet, “Playing with duality: An overview of recent primal-dual approaches for solving large-scale optimization problems,” *IEEE Signal Processing Magazine*, vol. 32, no. 6, pp. 31–54, 2015.
- [29] N. Yadati, M. Nimishakavi, P. Yadav, V. Nitin, A. Louis, and P. Talukdar, *HyperGCN: a new method of training graph convolutional networks on hypergraphs*. Red Hook, NY, USA: Curran Associates Inc., 2019.
- [30] “Lung cancer trends brief: Mortality,” American Lung Association. [Online]. Available: [https://www.lung.org/research/trends-in-lung-disease/lung-cancer-trends-brief/lung-cancer-mortality-\(1\)](https://www.lung.org/research/trends-in-lung-disease/lung-cancer-trends-brief/lung-cancer-mortality-(1))
- [31] “State tobacco activities tracking and evaluation (state) system,” Centers for Disease Control and Prevention. [Online]. Available: <https://nccd.cdc.gov/STATESystem/>
- [32] “Statewide mapping — climate at a glance,” National Centers for Environmental Information. [Online]. Available: <https://www.ncei.noaa.gov/access/monitoring/climate-at-a-glance/statewide/mapping>
- [33] “Lung cancer risk factors,” Centers for Disease Control and Prevention, 10 2024. [Online]. Available: <https://www.cdc.gov/lung-cancer/risk-factors/index.html>
- [34] J. O. Owuor, J. L. Munda, and A. A. Jimoh, “The ieeec 34 node radial test feeder as a simulation testbench for distributed generation,” *IEEE Africon ’11*, pp. 1–6, 2011. [Online]. Available: <https://api.semanticscholar.org/CorpusID:22656721>
- [35] K. P. Schneider, B. A. Mather, B. C. Pal, C.-W. Ten, G. J. Shirek, H. Zhu, J. C. Fuller, J. L. R. Pereira, L. F. Ochoa, L. R. de Araujo, R. C. Dugan, S. Matthias, S. Paudyal, T. E. McDermott, and W. Kersting, “Analytic considerations and design basis for the ieeec distribution test feeders,” *IEEE Transactions on Power Systems*, vol. 33, no. 3, pp. 3181–3188, 2018.
- [36] J. F. Martins, A. G. Pronto, V. Delgado-Gomes, and M. Sanduleac, “Chapter 4 - smart meters and advanced metering infrastructure,” in *Pathways to a Smarter Power System*, A. Taşçıkaraoğlu and O. Erdinç, Eds. Academic Press, 2019, pp. 89–114. [Online]. Available: <https://www.sciencedirect.com/science/article/pii/B9780081025925000041>